Thermodynamic evaluation of the Al_2O_3-Al_4C_3 system and stability of Al-oxycarbides

Caian Qiu and Rudi Metselaar

(Laboratory of Solid State Chemistry and Materials Science, Eindhoven University of Technology, P.O. Box 513, NL-5600 MB Eindhoven, The Netherlands)

Thermodynamic Evaluation of the Al_2O_3–Al_4C_3 System and Stability of Al-oxycarbides

Thermodynamic properties of the pseudo-binary Al_2O_3–Al_4C_3 system have been evaluated based on thermodynamic models. An ionic-liquid model was applied to the liquid slag phase and a compound-energy model to Al_2OC. Both the models are with two sublattices and the latter one can be extended to describe the solid solution phases formed among Al_2OC, AlN, and SiC. A description of the system was obtained and then used to calculate the Al_2O_3–Al_4C_3 phase diagram which shows satisfactory agreement with experimental observation. A series of potential diagrams was also calculated for the Al–C–O system, which illustrate the effect of partial pressures of Al, CO, and CO_2 gas on the stability of Al_4C_3, Al_2O_3, Al_4O_4C, and Al_2OC at different temperatures. These diagrams can provide an important basis for the carbothermic reduction of alumina to produce Al_4C_3.

1 Introduction

Chemical reactions in the Al–C–O system are the base for the carbothermic reduction of alumina (Al_2O_3) to produce Al-carbide (Al_4C_3). Al_4C_3 is now known as the only stable carbide in the binary Al–C system, and α-Al_2O_3 (simply denoted as Al_2O_3) as stable oxide in the binary Al–O system. Therefore, thermodynamic properties of the Al–C–O system and the phase diagram of the pseudo-binary Al_2O_3–Al_4C_3 system have become a subject of great interest for metallurgy and ceramic processing.

The diagram of the Al_2O_3–Al_4C_3 system was first constructed by Foster et al. [1] based on their experimental results, in which two Al-oxycarbides (Al_4O_4C with orthorhombic crystal structure and Al_2OC with hexagonal structure) were identified using chemical analysis and X-ray diffraction (XRD). Although some experiments [2 to 5] failed to produce Al_2OC, the existence of Al_2OC was confirmed by Lihrmann et al. [6] and Lefort et al. [7]. Lihrmann et al. further observed that Al_2OC remains stable only in the temperature range from 1730 to 1980 °C. At and below 1700 °C Al_2OC decomposes into Al_4O_4C and Al_4C_3. Consequently, they revised the diagram by adding an invariant equilibrium, $Al_2OC \rightarrow Al_4O_4C + Al_4C_3$, at a temperature between 1700 and 1730 °C. This result also suggests that Al_2OC should not be detected in a significant amount in an Al_2O_3 reduction cell which is usually conducted at about 1000 °C, and thus explains why Al_2OC could not be produced in the experiments [2 to 5]. Meanwhile, the reactions occurring in the ternary Al–C–O system have been analysed many times [2 to 5, 8 to 10]. Thermodynamic stability of Al_4C_3 and Al_2O_3 at various temperatures was also examined under certain partial pressures of different gas species [10]. Unfortunately, Al_4O_4C and Al_2OC were often excluded from analysis because of the lack of information on their thermodynamic properties.

Recently, the properties of the Al–C [11] and Al–O [12] systems have been assessed using thermodynamic models, and the stability of Al_4C_3 and Al_2O_3 are well described. The purpose of the present work is to evaluate the properties of the Al_2O_3–Al_4C_3 system from experimental information after combining the Al–C and Al–O systems. The effect of partial pressures of Al, CO, and CO_2 gas on the stability of the condensed phases at temperatures of practical interest will then be examined. The approach used in this work involves the thermodynamic models for the molar Gibbs energy of the various phases in the system.

2 Thermodynamic Models

2.1 Liquid Slag (LS)

The liquid slag in the Al–C–O system can be described by an ionic two-sublattice model [13] which assumes there is one sublattice for cation and another for anion, neutral species, and hypothetical vacancies. For the slag formed in the Al_2O_3–Al_4C_3 system, it is straightforward to treat it without introducing any neutral species and vacancies in the anion sublattice, i.e. $(Al^{3+})_P(C^{4-}, O^{2-})_Q$ where P and Q will vary with composition according to the following equations to maintain electroneutrality

$$P = \sum y_i(-v_i) = 4y_{C^{4-}} + 2y_{O^{2-}} \tag{1a}$$

$$Q = \sum y_i v_j = 3y_{Al^{3+}} = 3 \tag{1b}$$

Here the variables y_i and y_j are the so-called site fraction of the anion i and cation j in its sublattice, respectively. v_i represents the valency of the anion i and v_j the valency of the cation j. The molar Gibbs energy of the liquid slag (denoted as LS) is expressed as

$$G_m^{LS} = y_{C^{4-}} {}^{\circ}G^{LS}_{Al^{3+}:C^{4-}} + y_{O^{2-}} {}^{\circ}G^{LS}_{Al^{3+}:O^{2-}} + PRT\,(y_{C^{4-}} \ln y_{C^{4-}} + y_{O^{2-}} \ln y_{O^{2-}}) + {}^{E}G_m \tag{2}$$

where P is given by Eq. (1a), R is the gas constant, and T is the temperature in K. ${}^{\circ}G^{LS}_{Al^{3+}:O^{2-}}$ and ${}^{\circ}G^{LS}_{Al^{3+}:C^{4-}}$ are the molar Gibbs energy of Al_2O_3 and Al_4C_3 in the liquid state, respectively. The former is accepted from a previous study [12], the latter is described by using the congruent melting enthalpy (ΔH) and entropy (ΔS) for Al_4C_3

$${}^{\circ}G^{LS}_{Al^{3+}:C^{4-}} - {}^{\circ}G_m^{Al_4C_3} = \Delta H - T\,\Delta S \tag{3}$$

The enthalpy and entropy values and the Gibbs energy ($^\circ G_m^{Al_4C_3}$) of solid Al_4C_3 are presented in the Appendix according to the previous evaluation of the Al–C system [11]. Equation (3) is appropriate at the temperatures around the congruent melting point (2612 K) of Al_4C_3, but it will also be used at other temperatures due to the lack of experimental information on the difference of heat capacity between liquid Al_4C_3 and solid Al_4C_3. This treatment is the same as that applied to the liquid AlN [14] and liquid Si_3N_4 [15].

The last term ^EG_m in Eq. (2) denotes the excess Gibbs energy depending here on the interaction between C^{4-} and O^{2-} on the anion sublattice and is expressed as follows using a subregular model

$$^EG_m = y_{C^{4-}} - y_{O^{2-}} - [{}^0L + {}^1L(y_{C^{4-}} - y_{O^{2-}})] \quad (4)$$

The interaction parameters ^0L and ^1L for the slag are to be evaluated in this work.

2.2 Liquid Metal (LM)

The liquid Al with certain solubility of carbon and oxygen was modelled as a substitutional solution. Since the oxygen solubility in liquid Al is very small compared with the carbon solubility, oxygen can be neglected in the solution model for simplicity in the present case. Therefore, the previous description for the Al–C liquid phase [11] can be directly used in this work.

2.3 Al-carbide (Al_4C_3), Al-oxide (Al_2O_3), and Al-oxycarbides (Al_4O_4C, Al_2OC)

Al_4C_3, Al_2O_3, and Al_4O_4C are treated as stoichiometric phases with respect to their compositions. The thermodynamic descriptions of Al_4C_3 and Al_2O_3 have been obtained in previous evaluations [11, 12], whereas the molar Gibbs energy for Al_4O_4C is given by

$$^\circ G_m^{Al_4O_4C} = \frac{1}{3}\,^\circ G_m^{Al_4C_3} + \frac{4}{3}\,^\circ G_m^{Al_2O_3} + a_1 \quad (5)$$

where the molar Gibbs energy $^\circ G_m^{Al_4C_3}$ for Al_4C_3 and $^\circ G_m^{Al_2O_3}$ for Al_2O_3 are referred to the enthalpy (H^{SER}) of selected state at 298.15 K and 1 bar (10^5 Pa) denoted as SER (Stable Element Reference), as shown in the Appendix. The constant a_1 is to be estimated in this work.

Another Al-oxycarbide, Al_2OC, has the same crystal structure as AlN and SiC. This structure is based on the wurtzite-type lattice which consists of two hexagonal close packed (hcp) sublattices displaced from each other [16]. Recently, solid solution phases (denoted as 2H) with the same structure were observed in the Al_2OC–AlN–SiC system under certain circumstances [6, 17 to 20]. It can be presumed that the formation of the 2H phase results from the substitution between Al and Si atoms on metallic sites and substitution among C, N, and O atoms on non-metallic sites. As a consequence, a compound energy model [21] with two sublattices, i.e. $(Al^{3+}, Si^{4+})_2(C^{4-}, N^{3-}, O^{2-})_2$, is applied to describe the 2H phase, in which the fraction of cation and anion varies following a certain rule to maintain electroneutrality. This can be graphically illustrated by a triangular prism in Fig. 1, where the possible compositions fall on the neutral plane indicated by the shaded area. For Al_2OC, this model simply becomes $(Al^{3+})_2(C^{4-}, O^{2-})_2$ with $y_{C^{4-}} = y_{O^{2-}} = 0.5$, and its molar Gibbs energy is then obtained from

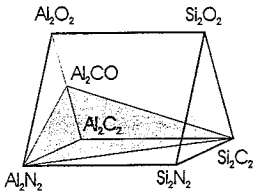

Fig. 1. Composition space for the solid solution (2H) formed among Al_2OC, AlN, SiC, where the possible compositions of the 2H phase fall on the neutral plane indicated by the shaded area.

$$^\circ G_m^{Al_2OC} = 0.5\,^\circ G_m^{Al_2C_2} + 0.5\,^\circ G_m^{Al_2O_2} + 2RT \ln 0.5 \quad (6)$$

Al_2C_2 and Al_2O_2 are hypothetical substances with the same structure as the 2H phase. Of the two unknown quantities of the molar Gibbs energy, $^\circ G_m^{Al_2O_2}$ is chosen as a reference here and set to zero. The other one, $^\circ G_m^{Al_2C_2}$, can be calculated from the Gibbs energy of Al_2OC which can also be expressed as follows

$$^\circ G_m^{Al_2OC} = \frac{1}{3}\,^\circ G_m^{Al_4C_3} + \frac{1}{3}\,^\circ G_m^{Al_2O_3} + a_2 + b_2 T + c_2 T \ln T \quad (7)$$

where the parameters a_2, b_2, and c_2 are to be determined from experimental information. The choices about the parameters in Eqs. (5) and (7) made in the present evaluation depend upon the amount of experimental information available.

3 Experimental Information and Parameter Evaluation

Foster et al. [1] reported the eutectic reaction (liquid → $Al_2O_3 + Al_4O_4C$) at about 1840 °C and the peritectic one (liquid + $Al_2OC \rightarrow Al_4O_4C$) at a temperature between 1870 and 1890 °C according to the observation of cooling curves and microstructure of samples. However, Ginsberg and Sparwald [3] and Gjerstad [4] gave a somewhat higher eutectic temperature around 1900 °C, which may be caused due to the failure of producing Al_2OC. The decomposition temperature for Al_2OC was found between 1700 and 1730 °C by Lihrmann et al. [6] who also suggested the peritectic melting temperature for Al_2OC to be close to 2000 °C. The eutectic composition was reported to be less than 11.8 mole% Al_4C_3 by Foster et al. based on their experiments, which essentially agrees with the observation by Lihrmann [22] who found an almost purely eutectic structure in the Al_2O_3–11.1Al_4C_3–6AlN and Al_2O_3–11.6Al_4C_3–5AlN (in mole%) samples after solidification. According to the above analysis, the results from [1, 6, 22] were used to evaluate the parameters stated in the preceding section. To assure that Al_2OC is not stable at and below 1700 °C, the following condition was introduced at temperatures below 1700 °C in the optimization

$$D = \frac{5}{8}\,^\circ G_m^{Al_4O_4C} + \frac{3}{8}\,^\circ G_m^{Al_4C_3} - {}^\circ G_m^{Al_2OC} < 0 \quad (8)$$

where the sum of the first two terms is the molar Gibbs energy of the equilibrium between Al_4O_4C and Al_4C_3 at $x_{Al_4C_3} = 0.5$, and thus D represents the driving force for the precipitation of Al_2OC from the equilibrium.

The liquidus temperatures were reported by Baur and Brunner [2] and by Ginsberg and Sparwald [3], but the values seem considerably high compared with the experimental observation [6] which indicated that the 82Al_2O_3–18Al_4C_3 sample (in mole%) was melted completely at 1950 °C. The latter information was taken into account in the optimization.

There are only few thermochemical measurements on the Al_2O_3–Al_4C_3 system. Motzfeldt and Sandberg [5] measured the pressures of carbon monoxide gas (CO) for the following reactions

$$2Al_2O_3 + 3C = Al_4O_4C + 2CO(g) \quad (9)$$

$$Al_4O_4C + 6C = Al_4C_3 + 4CO(g) \quad (10)$$

These data were included in the evaluation. However, similar measurements for reaction (9) by Cox and Midgeon [9] show much higher pressures of CO gas at the same condition and thus were not used. In the present study the gaseous phase was treated as the ideal gas including the following species: Al_1, Al_2, C_1, C_2, C_3, C_4, C_5, O_1, O_2, O_3, Al_1C_1, Al_1C_2, Al_2C_2, Al_1O_1, Al_1O_2, Al_2O_1, Al_2O_2, C_1O_1, C_2O_1, C_2O_2, C_3O_2. Their thermodynamic descriptions were taken from the SGTE substance database [23] which is mainly based upon the JANAF Table [24].

Having selected the experimental information from different sources as input data with a certain weight, the evaluation was made through an optimization program included in Thermo-Calc database [25]. The parameters were obtained in such a way that the calculation gives the best fit to most of the selected experimental data within expected uncertainty. During the course of this work, it was found that only one parameter, a_1 in Eq. (5), for Al_4O_4C can be determined due to lack of information on the stability of Al_4O_4C, whereas the parameters a_2, b_2, and c_2 in Eq. (7) can be determined very well with the help of the condition defined by Eq. (8). The present evaluation also showed that it was necessary to apply a subregular model to the liquid slag phase in order to have a better fit to the eutectic composition and temperature. In this case the interaction parameters ${}^0L$ and ${}^1L$ for the slag (see Eq. (4)) were treated as constants. All the thermodynamic parameters for the condensed phases are given in the Appendix which will be used to calculate the Al_2O–Al_4C_3 phase diagram and to examine the stability of Al-carbide, oxide, and oxycarbides under various conditions.

4 Results and Discussion

4.1 The Al_2O_3–Al_4C_3 Phase Diagram

The phase diagram calculated for the Al_2O_3–Al_4C_3 system without the gaseous phase is presented in Fig. 2 in comparison with experimental results [6]. The calculation shows that Al_4O_4C becomes stable from room temperature to 1870 °C at which it melts peritectically, whereas Al_2OC remains stable only within the temperature range from 1710 to 1990 °C. This agrees very well with the experimental observation. Other experimental data in Fig. 2 indicating the sample melted completely at 1950 °C were also accounted for by the present calculation. The calculated eutectic and peritectic temperatures for Al_4O_4C are close to the corresponding values reported by Foster et al. [1]. The eutectic composition is calculated to be 12.24 mole% Al_4C_3. That is the consequence after taking into account the experimental information on the Al_2O–Al_4C_3–AlN system [22]. This is illustrated in Fig. 3 which shows an Al_2O_3-rich corner of the projection calculated for the liquid slag, where each curve represents an invariant equilibrium and the arrows indicate decreasing temperature. Details on the calculation of the Al_2O_3–Al_4C_3–AlN system will be reported elsewhere [26]. There are two experimental samples observed to be almost purely eutectic structure after solidification and their compositions fall around the eutectic line extended from the binary system. Therefore, the liquidus curve calculated in equilibrium with Al_4O_4C or Al_2OC in Fig. 2 appears reasonable although it shows some disagreement with the experimental data on the liquidus temperatures [2, 3]. Above 2160 °C three phases (liquid metal, liquid slag, and graphite) co-exist in Fig. 2, because Al_4C_3 decomposes peritectically to carbon-saturated liquid metal and graphite, the compositions of which are outside the diagram. The calculated invariant equilibria are summarized in Table 1.

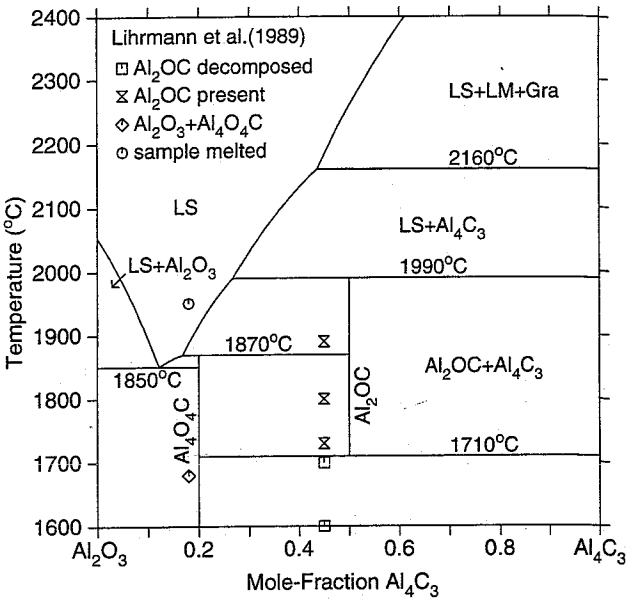

Fig. 2. Calculated phase diagram of the pseudo-binary Al_2O_3–Al_4C_3 system in comparison with experimental observation.

The calculated partial pressures of CO gas in the Al–C–O system with saturation of graphite are plotted as a function

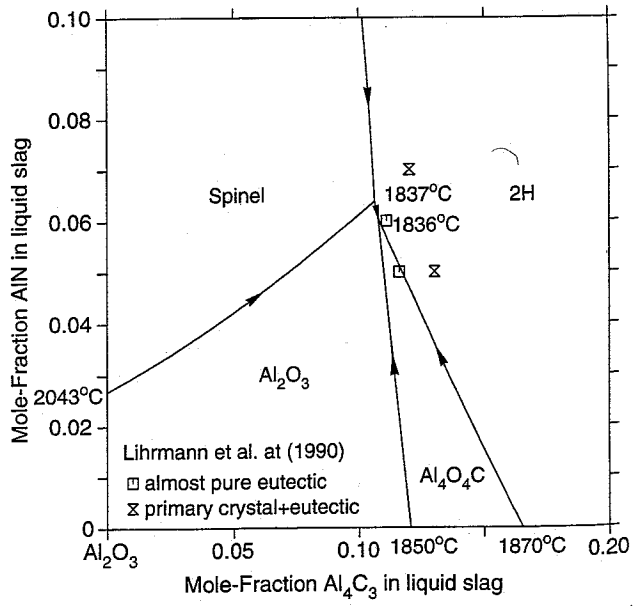

Fig. 3. Al_2O_3-rich corner of the projection calculated for the liquid slag in the Al_2O_3–Al_4C_3–AlN system compared with experimental results. The arrows indicate decreasing temperature during solidification.

Table 1. Calculated invariant equilibria in the Al_2O_3–Al_4C_3 system (LM – liquid metal; LS – liquid slag; Gra – graphite).

Equilibrium	Composition (mole% Al_4C_3)			Temperature (K)
$Al_2OC \rightarrow Al_4O_4C + Al_4C_3$ (eutectoid)	50	20	100	1983
$LS \rightarrow Al_2O_3 + Al_4O_4C$ (eutectic)	12.24	0	20	2123
$LS + Al_2OC \rightarrow Al_4O_4C$ (peritectic)	16.81	50	20	2143
$LS + Al_4C_3 \rightarrow Al_2OC$ (peritectic)	26.76	100	50	2263
$Al_2O_3 \rightarrow LS$ (congruent melting)	0	0	–	2227
$LM + Gra \rightarrow Al_4C_3$ (peritectic)	17.03 mole% C	100 mole% C	100	2433

of temperature in Fig. 4, compared with experimental measurements. The dashed line in Fig. 4 is extrapolated from the boundary between Al_4C_3 and Al_4O_4C and corresponds to reaction (10). There is reasonable agreement between the calculation and experiments for reaction (9), but the calculated pressures of CO gas fall slightly below the measured data for reaction (10). In addition, a disagreement in Fig. 4 was noticed between the calculation and experiments for the liquid slag phase. This was accepted since the properties of the slag were mainly evaluated from the eutectic temperature and composition.

4.2 Stability of Al_4C_3, Al_2O_3, Al_4O_4C, and Al_2OC

The calculated standard enthalpy, entropy, and Gibbs energy of formation of Al_4C_3, Al_2O_3, Al_4O_4C, and Al_2OC at 298.15 K are presented in Table 2. Among these the values for Al_4O_4C and Al_2OC should be regarded only as rough estimates. It is interesting to notice that the enthalpy values for Al_4O_4C and Al_2OC are of the same order of magnitude as the corresponding values calculated by Cox and Midgeon [9] from the enthalpy, entropy, and heat capacity of Al_2O_3 and Al_4C_3 after introducing certain assumptions.

Due to the presence of the gaseous phase in the Al–C–O system, it is particularly interesting for carbothermic reduction of alumina to examine the effect of partial pressures of

Table 2. Calculated molar enthalpy ($\Delta°H_m$), entropy ($\Delta°S_m$), and Gibbs energy ($\Delta°G_m$) of formation of Al_4C_3, Al_2O_3, Al_4O_4C, Al_2OC at 298.15 K. The values correspond to one mole of formula units.

Phase	$\Delta°H_m$ (kJ/mol)	$\Delta°S_m$ (J/mol/K)	$\Delta°G_m$ (kJ/mol)
Al_4C_3	−206.90	87.38	−232.95
Al_2O_3	−1675.69	50.94	−1690.88
Al_4O_4C	−2314.32[a])	97.05	−2343.25
Al_2OC	−634.96[a])	20.56	−641.09

[a]) The values are of the same magnitude as the corresponding enthalpy values (−2272.33 and −717.14) calculated by Cox and Midgeon [9].

different gas species on the stability of Al_4C_3, Al_2O_3, Al_4O_4C, and Al_2OC by using potential diagrams. Because such a process may be carried out at different temperatures, a series of potential diagrams was calculated for the Al–C–O system at temperatures between 1000 and 2000 °C and presented in Fig. 5 through Fig. 11 by using p_{CO_2} and p_{CO} as coordinates. The numbers in these diagrams represent invariant equilibria at a given temperature. In general, these diagrams show that p_{CO_2} is much lower than p_{CO}. Both p_{CO} and p_{CO_2} for the reaction involving Al_4O_4C and/or Al_2OC increase with increasing temperature. Especially, the stability of Al_2OC at 1800 °C as shown in Fig. 9 has been experimentally confirmed by Lefort et al. [7] who observed

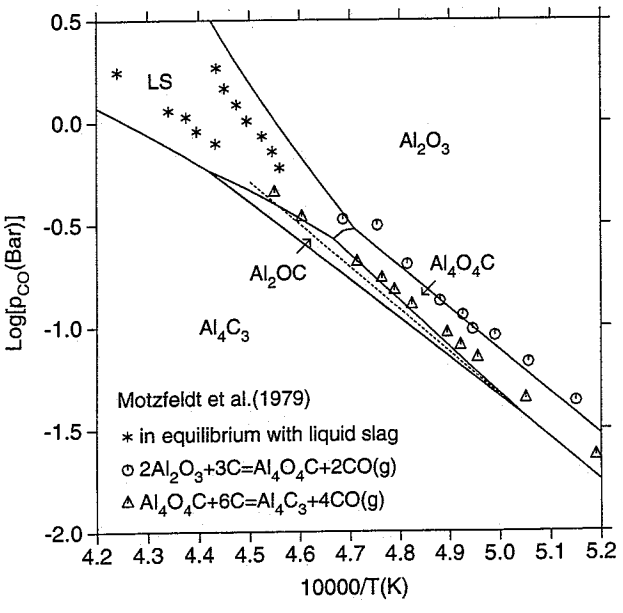

Fig. 4. Comparison between the calculated and measured partial pressures of CO gas as a function of temperature, where the dashed line is extrapolated from the boundary between Al_4C_3 and Al_4O_4C. All phases are in equilibrium with graphite.

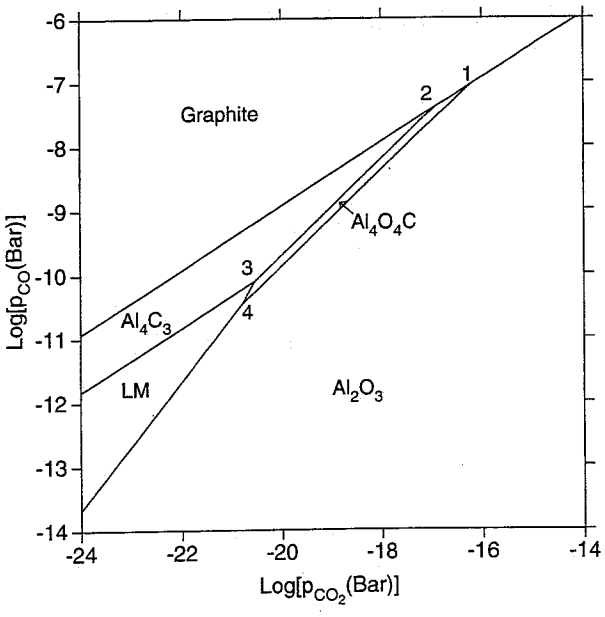

Fig. 5. Potential diagram of the Al–C–O system calculated at 1000 °C, where each number denotes an invariant equilibrium.

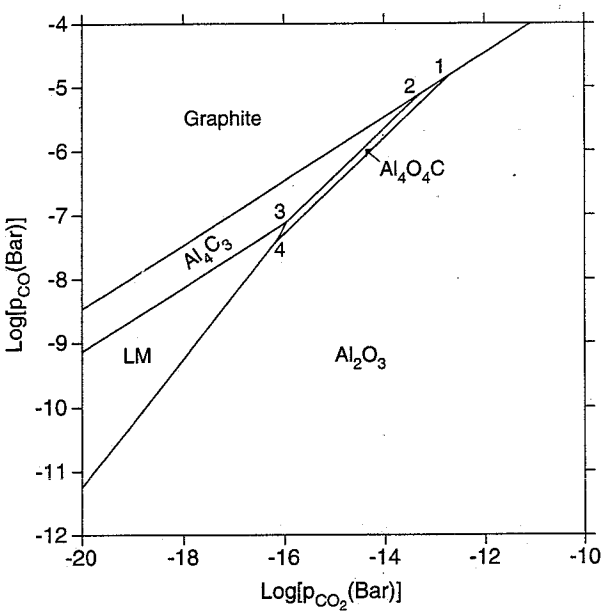

Fig. 6. Potential diagram of the Al–C–O system calculated at 1200 °C, where each number denotes an invariant equilibrium.

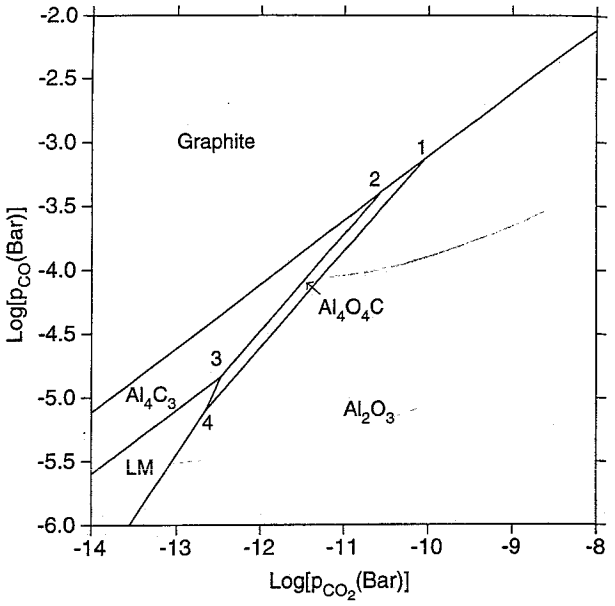

Fig. 7. Potential diagram of the Al–C–O system calculated at 1400 °C, where each number denotes an invariant equilibrium.

the formation of Al_2OC when heating a mixture of Al_2O_3 and graphite to 1800 °C under an imposed partial pressure 5000 Pa of CO gas. This is an encouragement to the present description of Al_2OC.

The calculated p_{CO} in the Al–C–O system is plotted as function of p_{Al} at different temperatures in Fig. 12a and b, where each invariant equilibrium at a given temperature is denoted with a number which corresponds to that shown in the previous diagrams. From Fig. 12 it can be seen that p_{Al} in the equilibrium between Al_4C_3 and graphite is independent of p_{CO}, and thus this equilibrium is represented by a vertical line. p_{Al} in the Al_4C_3/LM equilibrium and in the Al_2O_3/LM equilibrium varies little with p_{CO} at a given temperature, and its values are very close to each other at temperatures up to 1600 °C. As a result, the lines for the two equilibria almost overlap in Fig. 12a. However, at temperatures above 1600 °C the difference of p_{Al} for the two equilibria becomes evident as demonstrated in Fig. 12b. Since p_{CO} values for the invariant equilibria Al_4C_3/Al_2OC/LM and Al_2OC/Al_4O_4C/LM are almost equal at 1800 °C and also for Al_4C_3/LS/LM and Al_2OC/LS/LM at 1900 °C (see points 4 and 5 in Fig. 9 and Fig. 10), the corresponding equilibria overlap at 1800 and 1900 °C in Fig. 12b. Similar diagrams were found when using p_{CO_2} and p_{Al} as coordinates, as shown in Fig. 13a and b. Now it is noticed that points 4 and 5 no longer coincide at 1800 and 1900 °C in Fig. 13b.

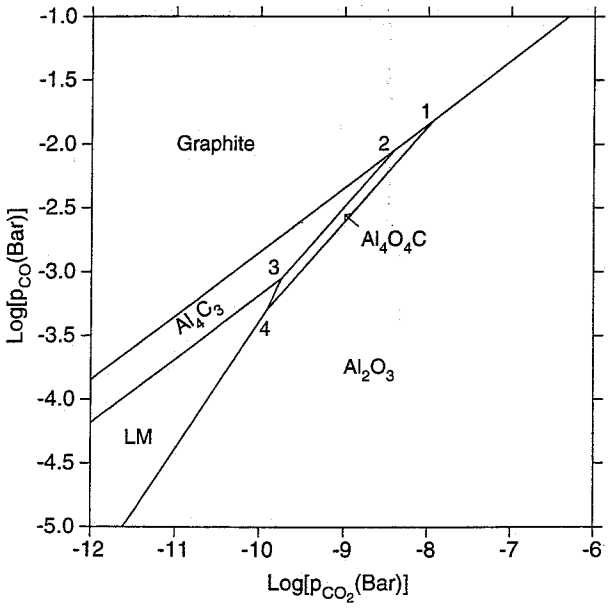

Fig. 8. Potential diagram of the Al–C–O system calculated at 1600 °C, where each number denotes an invariant equilibrium.

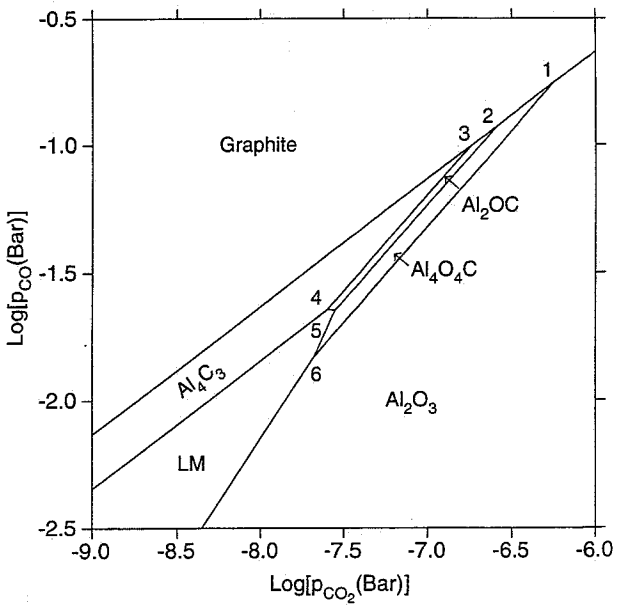

Fig. 9. Potential diagram of the Al–C–O system calculated at 1800 °C, where each number denotes an invariant equilibrium. The stability of Al_2OC is in agreement with experimental observation under p_{CO} = 5000 Pa [7].

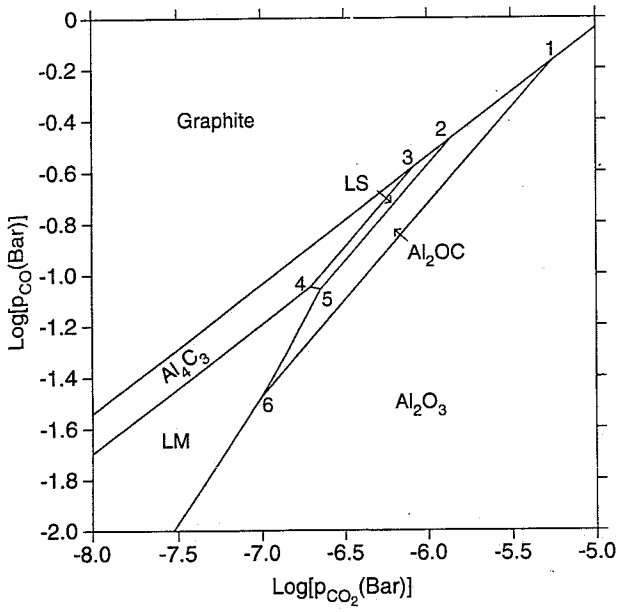

Fig. 10. Potential diagram of the Al–C–O system calculated at 1900 °C, where each number denotes an invariant equilibrium.

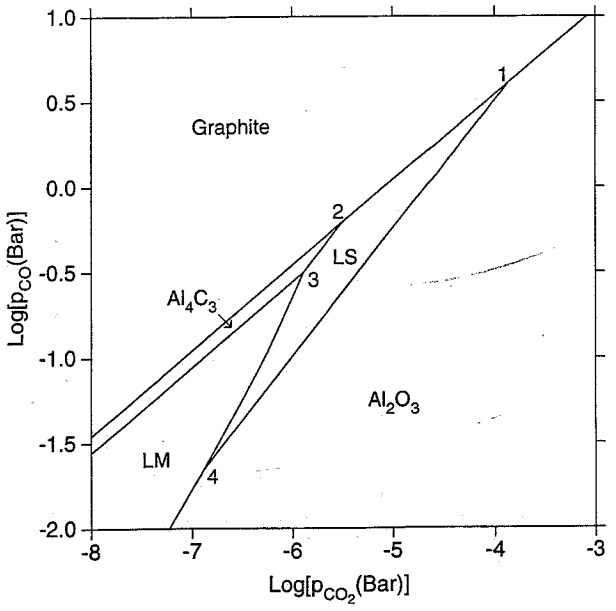

Fig. 11. Potential diagram of the Al–C–O system calculated at 2000 °C, where each number denotes an invariant equilibrium.

Such potential diagrams in the temperature range from 1000 K to 1800 K were also calculated by Morfopoulos [10] on the basis of stability criteria and stoichiometric reactions. However, he found Al_4O_4C and Al_2OC thermodynamically unstable in this temperature range and thus limited the analysis of the Al–C–O system to the phases other than Al-oxycarbides. Compared with his analysis, the potential diagrams presented in this work are considered as more complete and more reliable.

5 Summary and Conclusions

By taking experimental information into account, thermodynamic properties of the pseudo-binary Al_2O_3–Al_4C_3 system have been evaluated based on thermodynamic models. An ionic-liquid model and a compound-energy model were applied to the liquid slag and Al_2OC, respectively. The latter model can be extended to describe the solid solution phases formed among Al_2OC, AlN, and SiC. The calculated Al_2O_3–Al_4C_3 phase diagram is presented which shows satisfactory agreement with experimental observation.

A series of potential diagrams was calculated for the Al–C–O system at temperatures between 1000 and 2000 °C, which can be used to examine the effect of partial pressures of Al, CO, and CO_2 gas on the stability of the condensed phases at different temperatures. These diagrams can provide an important basis for the carbothermic reduction of alumina to produce Al_4C_3.

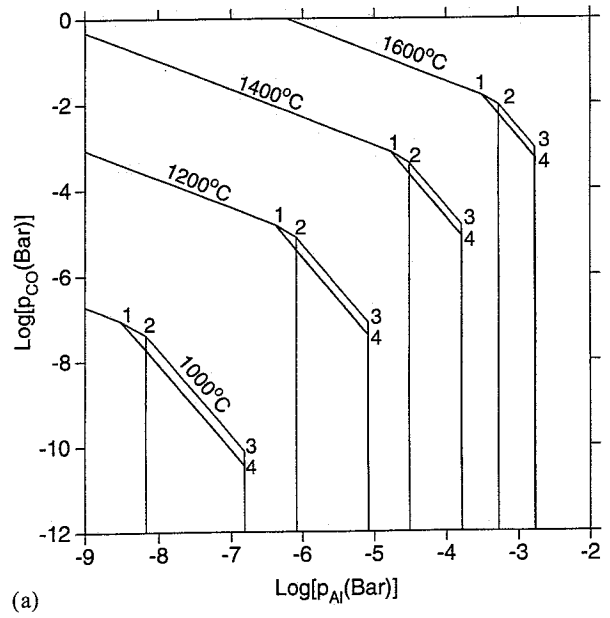

(a)

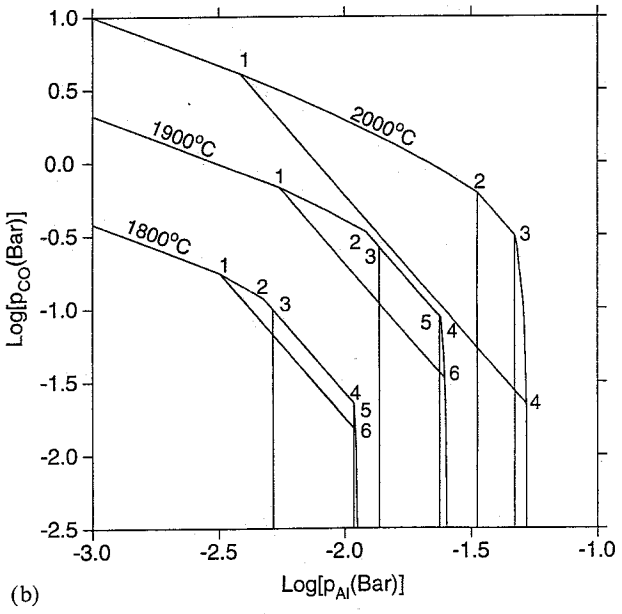

(b)

Fig. 12a and b. Potential diagram of the Al–C–O system calculated at (a) lower and (b) higher temperatures showing the variation of p_{CO} as function of p_{Al}, where numbers denote the same invariant equilibria as indicated in Fig. 5 through Fig. 11 at corresponding temperatures. Notice that points 4 and 5 almost coincide at 1800 and 1900 °C.

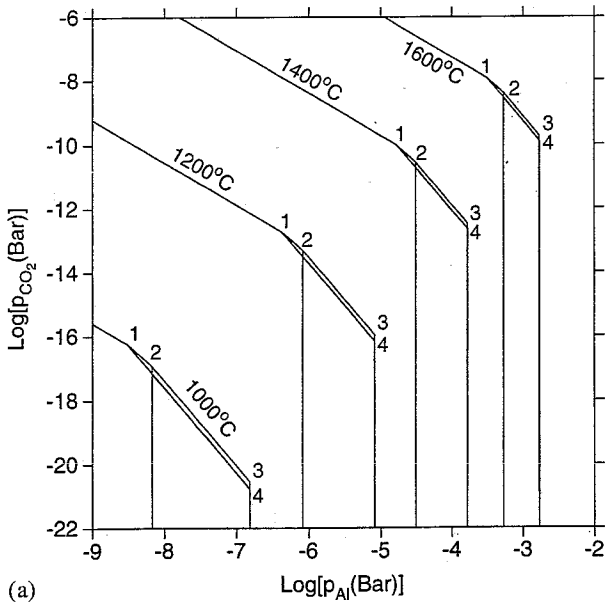

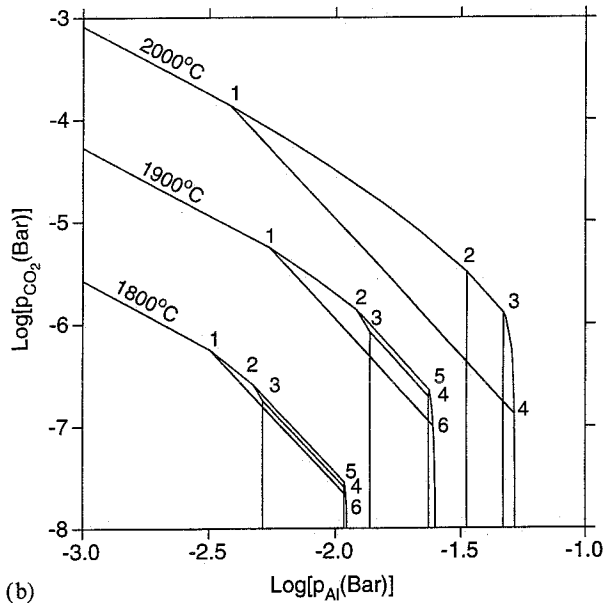

Fig. 13a and b. Potential diagram of the Al–C–O system calculated at (a) lower and (b) higher temperatures showing the variation of p_{CO_2} as function of p_{Al}, where numbers denote the same invariant equilibria as indicated in Fig. 5 through Fig. 11 at corresponding temperatures.

Useful comments on this article are acknowledged from Prof. F. J. J. van Loo and Dr. G. H. M. Gubbels. One of the authors (C. Qiu) would like to thank Eindhoven University of Technology for the financial support.

Appendix

Thermodynamic parameters for the condensed phases in the Al–C–O system. Values are given in SI units (J, mol, K) and correspond to one mole of formula units.

Solid Elements [27]

$298.15 < T < 700.00$

$$^{\circ}G^{fcc}_{Al} - H^{SER}_{Al} = -7976.15 + 137.093038\,T - 24.3671976\,T\ln T - 0.001884662\,T^2 - 8.77664 \times 10^{-7}T^3 + 74092/T$$

$700.00 < T < 933.60$

$$^{\circ}G^{fcc}_{Al} - H^{SER}_{Al} = -11276.24 + 223.048446\,T - 38.5844296\,T\ln T + 0.018531982\,T^2 - 5.764227 \times 10^{-6}T^3 + 74092/T$$

$933.60 < T < 2900.00$

$$^{\circ}G^{fcc}_{Al} - H^{SER}_{Al} = -11278.378 + 188.684153\,T - 31.748192\,T\ln T - 1.231 \times 10^{28}/T^9$$

$298.15 < T < 6000.00$

$$^{\circ}G^{gra}_{C} - {}^{\circ}H^{SER}_{C} = -17368.441 + 170.73\,T - 24.3T\ln T - 4.723 \times 10^{-4}T^2 + 2562600/T - 2.643 \times 10^{8}/T^2 + 1.2 \times 10^{10}/T^3$$

Liquid Metal (LM) with Formula (Al, C)$_1$ [11, 27]

$298.15 < T < 933.60$

$$^{\circ}G^{liq}_{Al} = {}^{\circ}G^{fcc}_{Al} + 11005.029 - 11.841867\,T + 7.934 \times 10^{-20}T^7$$

$933.60 < T < 2900$

$$^{\circ}G^{liq}_{Al} = {}^{\circ}G^{fcc}_{Al} + 10482.382 - 11.253975\,T + 1.231 \times 10^{28}/T^9$$

$298.15 < T < 6000$

$$^{\circ}G^{liq}_{C} = {}^{\circ}G^{gra}_{C} + 117369 - 24.63\,T$$

$$L^{liq}_{Al,C} = -4426 - 11.1007\,T$$

Liquid Slag (LS) with Formula $(Al^{3+})_P(C^{4-}, O^{2-})_Q$ [11, 12]

$$^{\circ}G^{LS}_{Al^{3+}C^{4-}} - 4H^{SER}_{Al} - 3H^{SER}_{C} = {}^{\circ}G^{Al_4C_3}_{m} + 587717 - 224.9837\,T$$

$298.15 < T < 600.00$

$$^{\circ}G^{LS}_{Al^{3+}O^{2-}} - 3H^{SER}_{Al} - 2H^{SER}_{O} = -1607850.8 + 405.559491\,T - 67.4804\,T\ln T - 0.06747\,T^2 + 1.4205433 \times 10^{-5}T^3 + 938780/T$$

$600.00 < T < 1500.00$

$$^{\circ}G^{LS}_{Al^{3+}O^{2-}} - 3H^{SER}_{Al} - 2H^{SER}_{O} = -1625385.57 + 712.394972\,T - 116.258\,T\ln T - 0.0072257\,T^2 + 2.78532 \times 10^{-7}T^3 + 2120700/T$$

$1500.00 < T < 1912.00$

$$^{\circ}G^{LS}_{Al^{3+}O^{2-}} - 3H^{SER}_{Al} - 2H^{SER}_{O} = -1672662.69 + 1010.9932\,T - 156.058\,T\ln T + 0.00709105\,T^2 - 6.29402 \times 10^{-7}T^3 + 12366650/T$$

$1912.00 < T < 2327.00$

$$^{\circ}G^{LS}_{Al^{3+}O^{2-}} - 3H^{SER}_{Al} - 2H^{SER}_{O} = 29178041.6 - 168360.926\,T + 21987.1791\,T\ln T - 6.99552951\,T^2 + 4.10226192\times10^{-4}T^3 - 7.98843618\times10^{9}/T$$

$2327.00 < T < 4000.00$

$$^{\circ}G^{LS}_{Al^{3+}O^{2-}} - 3H^{SER}_{Al} - 2H^{SER}_{O} = -1757702.05 + 1344.84833\,T - 192.464\,T\ln T$$

$$L^{LS}_{Al^{3+}:C^{4-},O^{2-}} = -12000 + 58000(y_{C^{4-}} - y_{O^{2-}})$$

Al_4C_3 [11]

$$^{\circ}G^{Al_4C_3}_{m} - 4H^{SER}_{Al} - 3H^{SER}_{C} = -265234 + 939.7257\,T - 148.7345\,T\ln T - 0.016733605\,T^2 + 3.63333333\times10^{-10}T^3 + 1863682/T$$

α-Al_2O_3 [12]

$298.15 < T < 600.00$

$$^{\circ}G^{Al_2O_3}_{m} - 2H^{SER}_{Al} - 3H^{SER}_{O} = -1707351.3 + 448.021092\,T - 67.4804\,T\ln T - 0.06747\,T^2 + 1.4205433\times10^{-5}T^3 + 938780/T$$

$600.00 < T < 1500.00$

$$^{\circ}G^{Al_2O_3}_{m} - 2H^{SER}_{Al} - 3H^{SER}_{O} = -1724886.06 + 754.856573\,T - 116.258\,T\ln T - 0.0072257\,T^2 + 2.78532\times10^{-7}T^3 + 2120700/T$$

$1500.00 < T < 3000.00$

$$^{\circ}G^{Al_2O_3}_{m} - 2H^{SER}_{Al} - 3H^{SER}_{O} = -1772163.19 + 1053.4548\,T - 156.058\,T\ln T + 0.00709105\,T^2 - 6.29402\times10^{-7}T^3 + 12366650/T$$

Al_4O_4C

$$^{\circ}G^{Al_4O_4C}_{m} = \frac{1}{3}\,^{\circ}G^{Al_4C_3}_{m} + \frac{4}{3}\,^{\circ}G^{Al_2O_3}_{m} - 11100$$

Al_2OC (2H) with Formula $(Al^{3+})_2$ $(C^{4-}, O^{2-})_2$

$$^{\circ}G^{2H}_{Al^{3+}:C^{4-}} = 0$$

$$^{\circ}G^{2H}_{Al^{3+}:O^{2-}} = 2\left(\frac{1}{3}\,^{\circ}G^{Al_4C_3}_{m} + \frac{1}{3}\,^{\circ}G^{Al_2O_3}_{m} - 14050 + 174.2368\,T - 22.20\,T\ln T\right) - 4\,RT\ln 0.5$$

Literature

1. *Foster, L. M.; Long, G.; Hunter, M. S.:* J. Am. Ceram. Soc. *39* (1956) 1–11.
2. *Baur, E.; Brunner, R.:* Z. Elektrochem. *40* (1934) 154–158.
3. *Ginsberg, H.; Sparwald, V.:* Aluminium *41* (1965) 181–230.
4. *Gjerstad, S.:* Thesis, Norges Tekniske Högskole, Trondheim, Dec. 1968. (also see [5]).
5. *Motzfeldt, K.; Sandberg, B.:* in: W. S. Peterson (ed.), Light Metals 1979, The Metallurgical Society of AIME, Warrendale, PA (1979) 411–428.
6. *Lihrmann, J. M.; Zambetakis, T.; Daire, M.:* J. Am. Ceram. Soc. *72* (1989) 1704–1709.
7. *Lefort, P.; Tetard, D.; Tristant, P.:* J. Europ. Ceram. Soc. *12* (1993) 123–129.
8. *Stroup, P. T.:* Trans. AIME *230* (1964) 356–372.
9. *Cox, J. H.; Midgeon, L. M.:* Can. J. Chem. *41* (1963) 671–683.
10. *Morfopoulos, V. C. P.:* Can. Metall. Q. *3* (1964) 95–116.
11. *Qiu, C.; Metselaar, R.:* J. Alloys and Compounds 1994 (in press).
12. *Taylor, J. R.; Dinsdale, A. T.; Hillert, M.; Selleby M.:* CALPHAD *16* (1992) 173–179.
13. *Hillert, M.; Jansson, B.; Sundman, B.; Ågren, J.:* Metall. Trans. A *16A* (1985) 261–266.
14. *Hillert, M.; Jonsson, S.:* Metall. Trans. A *23A* (1992) 3141–3149.
15. *Hillert, M.; Jonsson, S.:* Z. Metallkd. *83* (1992) 648–654.
16. *Amma, E. L.; Jeffrey, G. A.:* J. Chem. Phys. *34* (1961) 252–259.
17. *Cutler, I. B.; Miller, P. T.; Rafaniello, W.; Park, H. K.; Thompson, D. P.; Jack, K. H.:* Nature (London) *275* (1978) 434–435.
18. *Huang, J.-L.; Hurford, A.; Cutler, R. A.; Virkar, A. V.:* J. Mater. Sci. *21* (1986) 1449–1456.
19. *Kuo, S.-Y.; Virkar, A. V.; Rafaniello, W.:* J. Mater. Sci. *21* (1986) 3019–3024.
20. *Kuo, S.-Y.; Virkar, A. V.; J. Am. Ceram. Soc. 73* (1990) 2640–2646.
21. *Hillert, M.; Jansson, B.; Sundman, B.:* Z. Metallkd. *79* (1988) 81–87.
22. *Lihrmann, J. M.:* Proc. 11th Risø Int. Symp. on Structural Ceramics: Processing, Microstructure, and Properties, Roskilde, Denmark, Sept. 1990.
23. *Ansara, I.; Sundman, B.:* in: P. S. Glaser (ed.), Computer Handling and Dissemination of Data, North-Holland, Amsterdam (1987) 154–158.
24. JANAF Thermochemical Tables, Third Edition, M. W. Chase, Jr., C. A. Davis, J. R. Downey Jr., D. J. Furip, R. A. McDonald, A. N. Syverud (eds.), J. Phys. Chem. Ref. Data 14 (1985) Suppl. 1.
25. *Sundman, B.; Jansson, B.; Andersson, J.-O.:* CALPHAD *9* (1985) 153–190.
26. *Qiu, C.; Metselaar, R.:* unpublished research, Lab. of Solid Chemistry and Materials Science, Eindhoven University of Technology, The Netherlands, 1994.
27. *Dinsdale, A. T.:* CALPHAD *15* (1991) 327–415.

(Received May 2, 1994)